

GAZİ

JOURNAL OF ENGINEERING SCIENCES

## Charpy Impact Test in 3D-FDM and Optimization with Artificial Intelligence

Mehmet Altuğ<sup>\*a</sup>

Submitted: 22.11.2023 Revised: 26.12.2023 Accepted: 17.01.2024 doi:10.30855/gmbd.0705N02

### ABSTRACT

**Keywords:** FDM, Charpy impact test, Build orientation, Notch, Deep learning, Extreme learning machines

<sup>a</sup>Inonu University, Malatya OIZ Vocational School, Malatya / Türkiye  
Orcid: 0000-0002-4745-9164  
\*e mail: mehmet.altug@inonu.edu.tr

In the study, the rates of impact energy absorption of Acrylonitrile Butadiene Styrene (ABS) fractures produced by the Fused Deposition Modeling (FDM) method were examined. Charpy impact test results were determined using layer thickness, printing speed, support angle, build orientation, notch type, and unfill type. Box-behnken experimental design in the study. Notch impact samples are produced on an ABS Three-dimensional Printer (3DP). Then, Charpy impact tests were performed on the impact test device. Data were evaluated using the Minitab 21 program. Later, Deep Learning (DL) and Extreme Learning Machines (ELM) file models were created based on this development. The best results were obtained as 0.844 kJ/m<sup>2</sup> with a layer thickness of 0.09 mm. At 60 mm/s printing speed and 30° support angle, the impact energy absorption is 0.803 kJ/m<sup>2</sup>. The extinction edge of the highest impact energy is 0.841 kJ/m<sup>2</sup>. The most effective impact absorption was obtained as 0.827 kJ/m<sup>2</sup> in the U notch type. In the full infill type, impact energy absorption is obtained as 0.777 kJ/m<sup>2</sup>. In DL, tanh is the programming and tanh is the activation function. DL, Mean Squared Error (MSE) value was calculated as 0.000923, r<sup>2</sup> was calculated as 0.97427. In ELM, the activation function is sigmoidal at the input and linear at the output.

## 3D-FDM'de Charpy Darbe Testinin Yapay Zekâ ile Optimizasyonu

### ÖZ

Çalışmada FDM yöntemiyle üretilen ABS parçaların darbe enerjisi emilim oranları incelenmiştir. Charpy darbe testi sonuçları, katman dağılımı, yazdırma hızı, destek açısı, yapı yönü, çentik tipi ve dolgu tip kullanılarak belirlendi. Çalışmada Box-behnken deneysel tasarım tasarımı kullanıldı. Çentik darbe numuneleri 3D yazıcıda ABS malzemeden üretildi. Daha sonra darbe test cihazında Charpy darbe testleri yapıldı. Veriler Minitab 21 programı kullanılarak değerlendirildi. Daha sonra bu sonuçlara dayanarak DL ve ELM modelleri oluşturuldu. En iyi sonuçlar 0,09 mm katman kalınlığında 0,844 kJ/m<sup>2</sup>, 60 mm/s baskı hızında ve 30° destek açısında darbe enerjisi emilimi 0,803 kJ/m<sup>2</sup> olarak belirlendi. En yüksek darbe enerjisinin edge yönünde 0,841 kJ/m<sup>2</sup>, U çentik tipinde 0,827 kJ/m<sup>2</sup>, full dolgulu tipinde 0,777 kJ/m<sup>2</sup> olarak elde edildi. DL'de tanh optimizasyon algoritması, tanh ise aktivasyon fonksiyonudur. DL, MSE değeri 0,000923, r<sup>2</sup> ise 0,97427 olarak hesaplandı. ELM'de aktivasyon fonksiyonu girişte sigmoid, çıkışta ise doğrusaldır.

**Anahtar Kelimeler:** FDM, Charpy darbe testi, Konumlandırma, çentik tipi, Derin öğrenme, Aşırı öğrenme makineleri

## 1. Introduction

There are many researchers and studies working on Additive Manufacturing (AM) and Reverse Engineering (RE) related issues. Three-dimensional (3D) printing has brought some advantages in its own way. These are design flexibility, high precision and less material usage. FDM and polyjet are widely used in 3D printing methods. Since the mechanical, and rheological properties of the parts in additive manufacturing are relatively low, their printing potential is quite weak [1–4].

Pattnaik et al. He evaluated the advantages and disadvantages of the limitations in production sound in AM. Thus, it has been observed that high costs and long periods of time have been reduced in some critical sectors [5]. Anwer and his colleagues developed simulations with computer-aided tolerance systems to model the effects of tolerances [6]. Chiu et al. minimized the time required for repeatability fabrications by optimizing 3D fabrication parameters [7]. Alvarez et al. studied the effect of filler density on the impact and tensile strength of ABS samples [8]. Martinez-Garcia et al. surveyed the effect of different AM techniques on the mechanical properties of polymer parts. Some other researchers have investigated the dimensional and shape changes in Polyjet samples printed by different techniques [9]. In their study, Aroca and colleagues introduced 3D parts with a robot to enable low-cost mass production [10]. Cheng et al. They conducted a theoretical and experimental study for efficient optimization of the density of the cellular structure in AM [11].

Harynska et al. With the outstanding printability of Polylactic acid (PLA)/TPS, they investigated the characterization of self-produced bio-based PLA and TPS tailored for 3D printing technology [12]. Castro et al. They examined the mechanical properties of sandwich panels produced by AM [13]. Andrzejewski et al. investigated that the addition of TPS and PBAT greatly improved impact strength and elongation [14]. Tanveer et al. They studied the effect of filler density on the impact and tensile strength of PLA samples [15]. Caminero et al. They examined the effect of layer thickness on impact performance in nylon samples [16]. According to Feket et al., rubber was used to increase the ductility of PLA filaments and provide deformability compared to samples prepared using 3DPAF filler [17]. Korga et al. They studied the relationship between the percentage filling of the sample and the absorbed energy in AM [18]. Hadid et al. P430 investigated the effect of layer-by-layer shot peening on the low-speed impact properties of ABS parts and demonstrated high toughness and impact strength [19]. Sood et al. The effect of production parameters such as layer thickness and scanning angle on the mechanical properties of 3D parts produced by the FDM method was investigated and it was stated that they had an effect on the strength [20]. Ameri et al. the fracture behavior of 3D printed structures under dynamic loading conditions was investigated [21]. Hetrick et al. Investigated the effect of AM fabricated Kevlar fiber reinforced Onyx composites on impact energy absorption [22]. Kontárová et al. He worked on improving the mechanical and thermal properties of PLA-PHB mixtures [23]. Leon et al. Charpy tested polycarbonate and nylon+carbon fiber samples. According to the results, they found that the absorbed energy was higher for PA+CF material [24]. Velarde et al. They found that adding agave fibers to the filaments improved their crystallinity, impact strength and absorption values [25]. Ning et al. Tensile strengths of carbon fiber reinforced plastic composite parts produced by FDM method were examined and the effect of layer thickness on yield and tensile strength was examined [26]. Sa'ude et al. He investigated the mechanical properties of copper powder added ABS materials produced by FDM method and revealed that they had a significant positive effect [27]. Also ABS etc. There are other studies examining mechanical tests using polymer filaments [28–30]. These were made with different 3D printers and the results regarding mechanical properties were compared [31,32].

In the literature, there are many Deep Artificial Neural Network (ANN) studies involving convolutional neural networks (CNNs) created in computer vision and image recognition [33], [34] [35]. Ma et al. trained a deep convolutional neural network based on DeepLab. In their study, they applied a symmetric overlap-square strategy and a local processing method based on symmetric correction to increase the accuracy of the results with 3D information [36]. Oborski and Wysocki (2022) examined the quality control system with DL and revealed that the neural network created for visual quality control worked with 99.820% accuracy [37]. Lin et al. investigated to achieve high accuracy prediction performance using one-dimensional convolutional neural network, Fast Fourier Transform Long Short-Term Memory Network and Fast Fourier Transform-Deep Neural Networks. [38]. Pan et al. They worked on the accuracy rate of estimating surface roughness with deep learning [39]. Li et al. introduced a modeling approach to predict the  $R_a$  (surface roughness) of AM-produced parts. It has shown that 3D printed components can predict the surface roughness with high accuracy [40].

Dimitriou et al. they propose a system that automates diagnostics with ANN [41]. Yun et al. (2020) established a vision-based defect inspection system using defect images obtained from the metal production line. They stated that the proposed method showed an effective performance [42]. Zhang et al. presented a data-based prediction model with deep learning in the FDM method and stated that it performed better than other machine learning techniques [43]. Essien and Giannetti worked on the model consisting of DL and Deep convolutional LSTM encoder-decoder architecture [44]. Serin et al. have tried to monitor the team status with the DL method [45]. Wang et al. worked on a DL model for welding processes [46]. Cardoso et al. They stated that with the Machine Learning approach, useful results can be produced that will assist in providing appropriate resources, decision-making and operation of the system [47]. Klein et al. used random forests (RF) machine learning to estimate the size and surface quality characteristics of holes [48].

ELM was first introduced as a learning scheme for single-layer feedforward networks (SLFNs) and was stated to be able to estimate nonlinear function through random hidden neurons. In particular, the parameters of hidden neurons occur randomly and the activation function is a nonlinear continuous function. ELM was originally designed to solve the supervised learning problem. Later it is used in regression and classification problems [49–53]. The equation of a single hidden layer and feedforward neural network with  $n$  number of hidden nodes is shown as in Eq 2. The  $a_i$  and  $b_i$  in the equation are the learning parameters.  $B_i$ ,  $i$ . are the weights of the hidden node.  $G(x)$  is the activation function [49,50].

$$f_N(x) = \sum_{i=1}^N B_i G(a_i b_i x), x \in R, a_i \in R \quad (1)$$

Looking at the literature, ABS etc. There are also studies examining the mechanical properties of filaments. In this study, notch impact specimens were produced from ABS material in a 3D printer using the experimental design box behnken-RSM method in the first stage. Then, charpy tests were carried out on the AOB impact tester and statistical analyzes of all data obtained were performed in the Minitab 21 program. A model was created with DL and ELM methods through the data obtained in the second stage.

When the literature is examined, there are studies examining the mechanical properties of ABS etc. filaments. In the first stage of this study, notch impact specimens were produced from ABS material on a 3D printer. In the production of these specimens, the Response Surface Methodology (RSM)-Box behnken method, which is rarely encountered in the literature on the mechanical properties of filaments, was used as an experimental design. In addition, another important point that stands out differently from the literature is that AI models were created with DL and ELM methods depending on the data obtained in the experimental results.

## 2. Material and Methods

Box-Behnken RSM method, one of the surface response methods, was used in the study. Box-Behnken presents a data-driven relationship between the independent variable and the response function. In this context, the model is a first-order model if it shows a predictive result on the response surface as a linear func. of the independent variables (Equation 2). In case of degree of curvature in the response surface, it is a second-order model as in Equation 3.

$$y = \beta_0 + \beta_1 x_1 + \beta_2 x_2 + \dots + \beta_k \beta_k + \varepsilon \quad (2)$$

$$y = \beta_0 \sum_{i=1}^n \beta_i X_i + \sum_{i=0}^n \beta_{ii} X_i^2 + \sum_{i=0}^n \sum_{j=1}^n \beta_{ij} X_i X_j + \varepsilon_0 \quad (3)$$

(Table 1) below presents additive manufacturing parameters and levels. The results were analysed in Minitab 21 software. Sample production according to the parameters was made using the FDM method on a Zortrax M200 (Figure 1) 3D printer. Charpy impact specimens were fabricated using layer thickness, print speed, support angle as continuous factors and build orientation, notch type and filler type as categorical factors (Table 1). Here, the levels of 0.09 mm, 0.14 mm and 0.19 mm were selected for layer thickness on the 3D printer. For printing speed, 40, 60 and 80 mm/s, for support angle 20, 30 and 40 were selected. These choices were made by considering the literature. In the same way, flat, edge and upright production build orientation were selected for build orientation (Fig. 2a). The notch type, which is another important parameter of the study, was selected as U, V and Kh (Figure 2b), and full and mesh methods were selected for the fill type. ABS was used as the filament material. Charpy

impact test specimens (Figure 2) were produced in conformity with ASTM 6110 standard. Charpy impact energy were performed 1J on the AOB impact test device (Figure 3a) and the test sample and post-test sample status are given (Figure 3b).

Table 1. Box-behnken parametres and levels

Continuous Factors	Level values	
	Low	High
Layer thickness (mm)	0,09	0,19
Print speed (mm/s)	40	80
Support angle (°)	20	40

Categorical Factors	Level values		
	1.	2.	3.
Build Orientation	Flat	Edge	Upright
Notch type	V	U	Kh
Infill type	Full	Mesh	

After obtaining the experimental data, artificial intelligence based DL and ELM models were tried to be created. recommended prediction model was created with ELM and DL for the Charpy impact test data. Artificial intelligence based analyses of the results were realised in Anaconda-Python 3.9.



Figure 1. 3D printer in the study

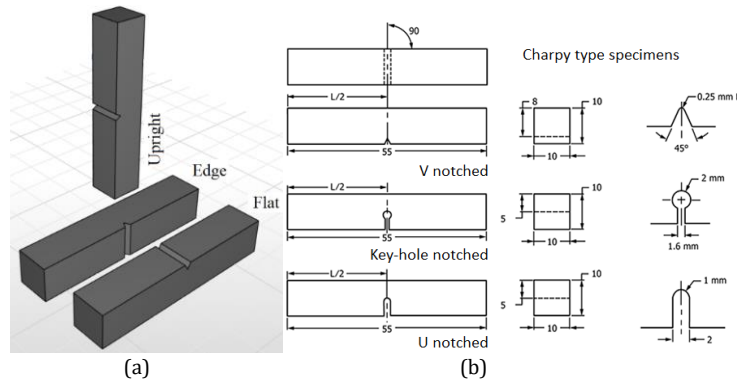


Figure 2. Charpy impact test specimens a) build orientations b) notch type



Figure 3. a) Charpy impact test device in the study and b) samples

### 3. Results and Discussion

#### 3.1 Response surface method (RSM)

This study, which was measured with the RSM method, the Box behnken method was used as the design of experiment (DOE). In accordance with this experimental design, notch impact samples were produced on the 3D printer. Charpy tests were performed on a Shimadzu brand impact tester and all the data obtained were processed (Table 2). The data achieved after the charpy test were analyzed in Minitab-21 software. Box-benhken analysis and Analysis of Variance (ANOVA) test were performed here. Additionally, figures and graphs were drawn to explain this study more effectively.

Table 2. Box-behnken design and results

Run Order	Pt Type	Blocks	Layer thickness (mm)	Print speed (mm/s)	Support angle (°)	Build orientation	Notch type	Infill type	Data (kJ/m <sup>2</sup> )
1	2	1	0,19	80	30	Edge	V	Mesh	0,539
2	2	1	0,14	40	20	Upright	Kh	Mesh	0,451
3	2	1	0,09	60	40	Edge	Kh	Full	0,951
4	2	1	0,14	40	20	Edge	V	Full	0,660
5	2	1	0,09	60	20	Edge	V	Mesh	0,724
6	2	1	0,09	80	30	Edge	V	Mesh	0,736
7	2	1	0,19	60	40	Upright	U	Mesh	0,636
.	.	.	.	.	.	.	.	.	.
.	.	.	.	.	.	.	.	.	.
.	.	.	.	.	.	.	.	.	.
264	2	1	0,19	60	20	Flat	U	Mesh	0,657
265	2	1	0,09	60	20	Edge	Kh	Full	0,973
266	2	1	0,14	80	40	Upright	Kh	Full	0,517
267	2	1	0,09	40	30	Edge	U	Mesh	1,081
268	2	1	0,14	80	40	Upright	U	Full	0,622
269	2	1	0,14	40	40	Flat	U	Mesh	0,726
270	2	1	0,09	80	30	Edge	Kh	Full	0,984

The effects of continuous and categorical parameters on the charpy impact test are demonstrate in (Figures 4&5). The impact strength data is inversely proportional to the layers thickness. It was concluded that the main reason behind this is that the smaller the diameter of the filament at the nozzle exit, the stronger the adhesion will be, as the surface area of adhesion to the previous layers will increase. Also, a thinner filament will create a tighter texture. In terms of charpy impact energy absorption, the high-odrer value charpy impact energy absorption was achieved with a layer thickness of 0.09 mm. In terms of layer thickness, the lowest impact energy absorption values were obtained at a layer thickness of 0.19 mm. The highest impact energy value absorption was obtained as 0.844 kJ/m<sup>2</sup> at 0.09 mm layer thickness. The results regarding the layer thickness are compatible with the searches in the literature [32,54,55].

When the effects of print speed on the charpy impact test data were commented and seen that most noteworthy results was at the median value of 60 mm/s. It was concluded that the main reason behind this is that the slow and fast writing process affects the adhesion and therefore the impact test value due to the cooling of the surface. The maximal charpy impact energy absorption was obtained as 0.803 kJ/m<sup>2</sup> at 60 mm/s printing speed. The results regarding the layer thickness are compatible with the

searches in the literature [54,55].

When the support angle values were commented and seen that the best outcomes were achieved at 30° degrees. The difference between the support angle of 20° and 40° with the filament reveals the fact that the adhesion decreases. The highest charpy impact energy absorption was obtained as 0.803 kJ/m<sup>2</sup> at 60 mm/s printing speed.

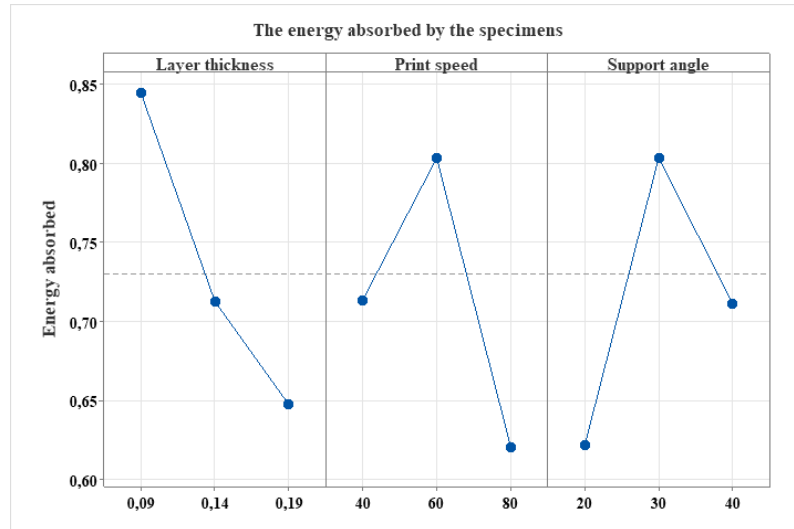


Figure 4. Main effects plot for continuous parameters

When the effect of categorical parameters is examined in Fig. 5, it gave extremely good results on the edge charpy impact test data from the build orientation values. Here, when the build orientation is considered together with the notch type, the edge gave good results because it is the surface that meets the impact load. Flat positioning followed this. Upright, where the samples were produced vertically, gave the weakest impact values due to both the oscillations during production and the elevation on a low cross-sectional area. The maximal charpy impact energy absorption was obtained as 0.841 kJ/m<sup>2</sup> at edge position. The results regarding the build orientation are compatible with the searches in the literature [22,29,56].

When notch type was examined, the highest charpy impact values were obtained in U type samples. This result can be explained as U-section absorbs the impact force by spreading it over a wide surface. The keyhole cutout also gave relatively good results. Again, the section where the impact force is distributed has gained importance here as well. The highest impact energy absorption was obtained as 0.827 kJ/m<sup>2</sup> at U notch type. The results regarding the layer thickness are compatible with the searches in the literature [18].

When the filling type is examined, as expected, the full filling type revealed the best results compared to the mesh filling type. The highest impact energy absorption was obtained as 0.777 kJ/m<sup>2</sup> at full infill type. The results regarding the layer thickness are compatible with the searches in the literature [18,22].

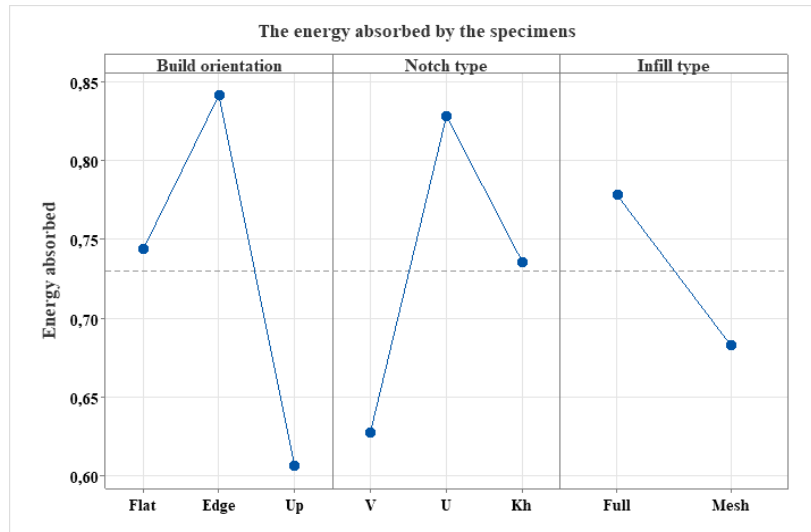


Figure 5. Main effects plot for categorical parameters

The  $r^2$  value of the model emerging with the Box-behnken method is 0.9529. However, the estimated and adjusted  $r^2$  values were revealed as 0.9454 and 0.9377. These numerical results demonstrated that there is a statistical highly remarkable fit in the box behnken model (Table 3).

Table 3. Model R results

S	R:sq	R:sq(adj)	R:sq(pred)
0,0453935	95,29%	94,54%	93,77%

ANOVA after charpy test is presented in (Table 4). The F result of the model obtained in ANOVA was 126.81 and a remarkable effect rate of 95.29% was obtained. In addition, with p values of the model being  $<0.05$ , it was unveiled that the model was statistically significant in terms of both linear and square values, with all continuous and categorical variables. According to ANOVA, the most effective parameters on the charpy results were build direction (24.69%) and notch type (17.81%).

Table 4. ANOVA for Process Parameters

Source	DF	Adj:SS	Adj:MS	F:Value	P:Value	Contribution
Model.	37	9,6682	0,26130	126,81	0,000	95,29%
Linear.	8	6,9118	0,86398	419,29	0,000	68,12%
Layer thickness	1	1,3926	1,39260	675,83	0,000	13,73%
Print speed	1	0,3111	0,31109	150,97	0,000	3,07%
Support angle	1	0,2878	0,28783	139,69	0,000	2,84%
Build orientation	2	2,5055	1,25277	607,97	0,000	24,69%
Notch type	2	1,8066	0,90331	438,38	0,000	17,81%
Infill type	1	0,6081	0,60814	295,13	0,000	5,99%
Square	3	2,7054	0,90179	437,64	0,000	26,66%
Layer thickness*Layer thickness	1	0,0100	0,00995	4,83	0,029	0,73%
Print speed*Print speed	1	1,4164	1,41642	687,39	0,000	11,96%
Support angle*Support angle	1	1,4178	1,41777	688,05	0,000	13,97%
2-Way Interaction	26	0,0510	0,00196	0,95	0,536	0,50%
Layer thickness* Print speed	1	0,0003	0,00028	0,14	0,713	0,00%
Layer thickness* Support angle	1	0,0023	0,00235	1,14	0,287	0,02%
Layer thickness* Build orientation	2	0,0019	0,00096	0,46	0,629	0,02%
Layer thickness* Notch type	2	0,0009	0,00044	0,21	0,807	0,01%
Layer thickness*Infill type	1	0,0000	0,00000	0,00	0,975	0,00%
Print speed*Support angle	1	0,0046	0,00462	2,24	0,135	0,05%
Print speed*Build orientation	2	0,0061	0,00307	1,49	0,227	0,06%
Print speed*Notch type	2	0,0118	0,00590	2,86	0,059	0,12%
Print speed*Infill type	1	0,0024	0,00236	1,15	0,286	0,02%
Support angle*Build orientation	2	0,0034	0,00169	0,82	0,441	0,03%
Support angle*Notch type	2	0,0004	0,00020	0,10	0,907	0,00%
Support angle*Infill type	1	0,0006	0,00059	0,29	0,592	0,01%
Build orientation*Notch type	4	0,0012	0,00030	0,15	0,965	0,01%
Build orientation*Infill type	2	0,0133	0,00667	3,24	0,041	0,13%
Notch type*Infill type	2	0,0017	0,00086	0,42	0,659	0,02%
Error	232	0,4781	0,00206			4,71%
Lack-of-Fit	196	0,3451	0,00176	0,48	0,999	3,40%
Pure Error	36	0,1329	0,00369			1,31%
Total	269	10,1462				100,00%

### 3.2 Optimization with artificial intelligence (AI)

Using these experimental data, ELM and DL prediction models were created. Before starting the analysis, dependent variables were not normalized, but independent variables were normalized in the [0,1] range. Normalization was applied to the data in both methods (DL and ELM). Sigmoid was applied as activation function in ELM. In ELM, the number hidden layer is set as 1. Eight different values were set for the number of neurons in the hidden layers (Table 5). 90% of the data was utilised for training the models and the of those who remain 10% was reserved for testing (Table 5). In DL, adam and rmsprop were applied as optimization algorithms, tanh, sigmoid and relu were applied as activation functions. In DL, the number of hidden layer is 3 and the number neurons in each hidden layer is 6 and 12. In DL, as in ELM, 90% of the data was utilised for training the models and the of those who remain 10% was reserved for testing. Epochs was set to 1000 (Table 5).

Table 5. DL and ELM parameters

AI Parameters	DL	Basic ELM	P/ELM	OP/ELM
Optimization Algorithms	Adam and Rmsprop	-	-	-
Normalization method	Min/Max Scaling	Min/Max Scaling	Min/Max Scaling	Min/Max Scaling
Activation Function for Input Layer	Relu, tanh, sigmoid	sigmoid	sigmoid	sigmoid
Activation Function for Output Layer	-	linear	linear	linear
Input Layer Neurons	6	6	6	6
Output Layer Neurons	1	6	6	6
Hidden Layers	3	1	1	1
Hidden-1 Layer Neurons	6;12	6;12;18;24	30;60;90;120	30;60;90;120
Hidden-2 Layer Neurons	6;12	-	-	-
Hidden-3 Layer Neurons	6;12	-	-	-
DL Learning Rate	0,001			
Batch Size	16			
Training data size	0,9	0,9	0,9	0,9
Test data size	0,1	0,1	0,1	0,1
Epochs for DL	1000	-	-	-

In this AI analysis, 96 trial runs were performed with DL parameters and 45 trial runs were performed with ELM parameters. The architectures of the AI (DL and ELM) models proposed as a result of these runs are presented in (Figures 6&7).

The max. dynamic results of DL were determined by the mean square error. Here, the best results were obtained under the following conditions. Adam as the optimization algorithm, tanh as the activation function, the number of hidden layers 3 and the number of neurons 6, 6 and 6. The architectural design of the DL model is shown in (Figure 6).

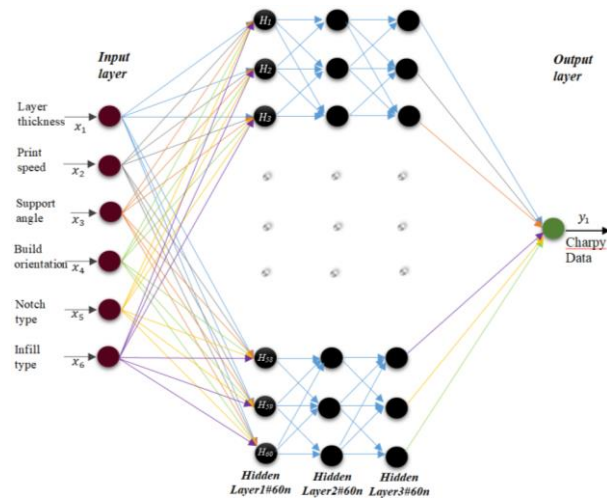


Figure 6. DL architecture of this study

The ELM model used in the research is demonstrated in (Figure 7). In ELM, the activation function is sigmoid at the input layer and linear at the output. In ELM, the best MSE results were obtained with 180 neurons in the hidden layer Optimally Pruned Extreme Learning Machine (OP-ELM).

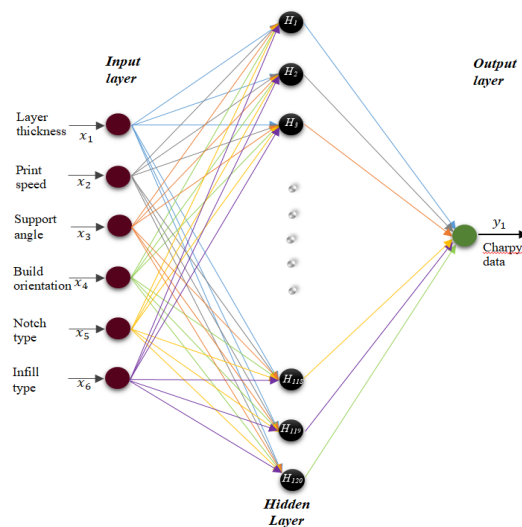


Figure 7. ELM architecture of this study

In this study, prediction models for ELM and DL were created using the Charpy test. The optimal MSE value in ELM was calculated as 0.00173 and  $r^2$  value as 0.96178. These results were obtained by using OP-ELM as the optimization algorithm and sigmoid as the activation function. The best MSE value in DL was calculated as 0.000923, and the  $r^2$  as 0.974274. These results were obtained using adam as the optimization algorithm and tanh as the activation function. Some of the other activation functions were also tried in ELM. However, since remarkable results are usually obtained in the sigmoid function, the results of other activation functions were not taken into account. Therefore, sigmoid was included in all ELM trials. All results are demonstrated in (Table 6).

For the models presented in this study, it is demonstrated that both DL and ELM give very successful prediction results as efficient optimization, although DL results are relatively better. The proper choice of model for further research and analyses will vary depending on the data set and print parameters.

Depending on the results obtained, it has revealed that that different artificial intelligence optimization practice can be applied in optimizing the outputs obtained with different parameters. More importance, it has become clear that AI-based optimizations give remarkable predictions as all the results obtained in additive manufacturing.

Table 6. Result of DL and ELM

	Method	Optimization algorithms	Neuron Number	Activation function	MSE Training	MSE Test	r <sup>2</sup>		
Charpy data (Kj/m <sup>2</sup> )	Deep Learning	Adam	(6,6,6)	Relu, Relu, Relu	0,014889	0,008906	0,78231		
				Sigm., Sigm., Sigm.	0.018986	0.014021	0.609101		
				tanh, tanh, tanh	0.001104	0.000923	<b>0.974274</b>		
			(6,12,12)	Relu, Relu, Relu	0,001835	0,004677	0,88568		
				Sigm., Sigm., Sigm.	0.01895	0.013402	0.626372		
				tanh, tanh, tanh	0.001177	0.001948	0.945683		
				Relu, Relu, Relu	0,00273	0,006389	0,84384		
				Sigm., Sigm., Sigm.	0.015924	0.012803	0.643054		
				tanh, tanh, tanh	0.00096	0.001744	0.951383		
			(12,6,6)	Relu, Relu, Relu	0,001431	0,005228	0,87221		
				Sigm., Sigm., Sigm.	0.017581	0.012305	0.656941		
				tanh, tanh, tanh	0,000768	0,001786	0,95020		
				Relu, Relu, Relu	0,009848	0,011644	0,7154		
				Sigm., Sigm., Sigm.	0.018496	0.014314	0.60093		
				tanh, tanh, tanh	0.003434	0.003451	0.903795		
			RmsProp	(6,12,12)	Relu, Relu, Relu	0,008579	0,010829	0,73532	
					Sigm., Sigm., Sigm.	0.01887	0.014302	0.601273	
					tanh, tanh, tanh	0.002399	0.00294	0.918035	
					Relu, Relu, Relu	0,002074	0,003994	0,90237	
					Sigm., Sigm., Sigm.	0.017955	0.012302	0.657039	
					tanh, tanh, tanh	0.001972	0.002593	0.927714	
				(12,12,12)	Relu, Relu, Relu	0,002517	0,010966	0,73196	
					Sigm., Sigm., Sigm.	0.019488	0.01361	0.620579	
					tanh, tanh, tanh	0,003791	0,004205	0,88277	
					6		0.014242	0.012677	0.646567
					12		0.012794	0.012072	0.663446
					18	Sigmoid	0.007343	0.003898	0.891334
			Extreme Learning Machines	Basic ELM	24		0.009754	0.010598	0.704544
					48		0.001341	0.002177	<b>0.94304</b>
					30		0.006035	0.007112	0.801723
					60		0.001037	0.002518	0.929812
					90	Sigmoid	0.001004	0.002458	<b>0.94548</b>
					120		0.001161	0.003248	0.909447
				OP-ELM	180		0.002334	0.003001	0.916346
					30		0.006506	0.00452	0.873975
					60		0.001254	0.002273	0.936618
90	Sigmoid	0.000908			0.004553	0.873054			
120		0.000539			0.002201	0.938638			
180		0.000563			0.00173	<b>0.96178</b>			

Comparisons of the predicted values achieved in the ELM and DL models with the values achieved in the experiments are displayed in (Figures 8&9). In the graphs, Red-dashed line demonstrate the predicted data of the best model, and black-solid line demonstrate the actual data. When figures are analyzed in detail, the data of the proposed models revealed results very close to the original data.

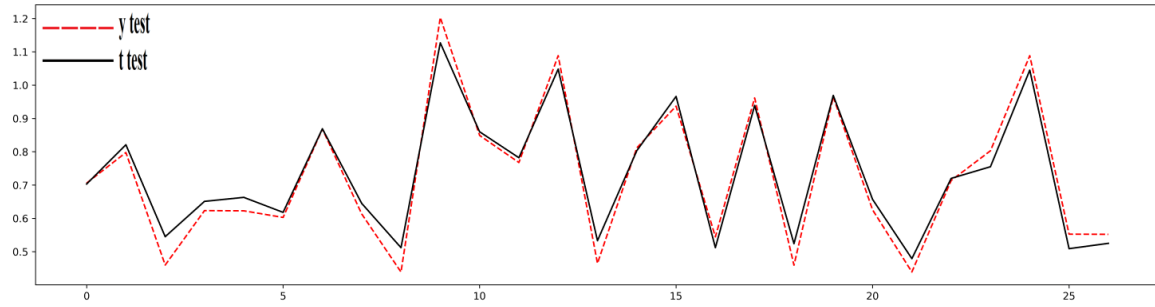


Figure 8. DL's original data vs. model output comparison chart in terms of best test MSE Value

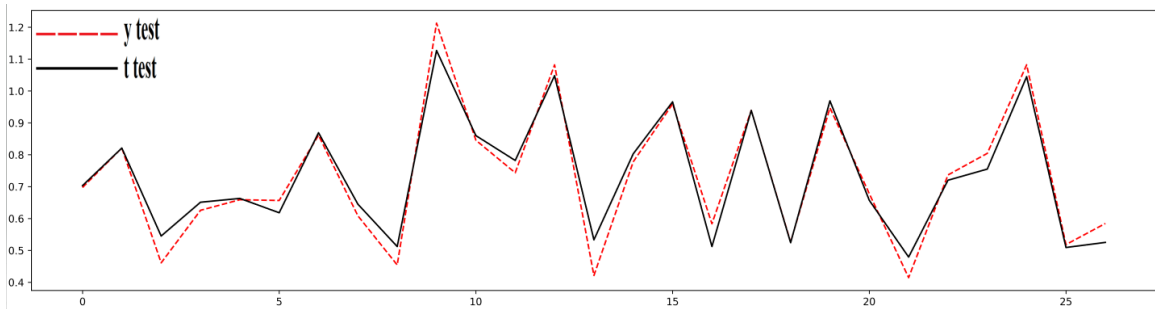


Figure 9. OP-ELM's original data vs. model output comparison chart in terms of best test MSE Value

## 4. Conclusion

In the study, Charpy impact tests were investigated out to determine the energy absorption of the specimens produced by the 3D-FDM method. In this study, notch impact specimens were produced from ABS material in a 3D printer using the experimental design box behnken RSM method in the first stage. Then, Charpy tests were performed on the AOB brand impact tester and all the data achieved were analyzed in the Minitab-21 software program. In the context of these conclusions achieved in the next stage, a model is presented with DL and ELM methods from these data. All the conclusions of the research are as follows;

- Charpy impact test data decreased with the increase in layer thickness values. A thinner filament is expected to produce a tighter texture. Among all experiments, the maximal Charpy impact energy absorption was obtained as  $0.844 \text{ kJ/m}^2$  at a layer thickness of  $0.09 \text{ mm}$ .
- The effects of printing speed on the Charpy impact test data were analysed and It has been seen that the best impressive result was obtained at  $60 \text{ mm/s}$ . It is thought that the slow and fast printing process affects the adhesion and thus the impact test value due to the cooling of the surface. The maximal Charpy impact energy absorption was obtained as  $0.803 \text{ kJ/m}^2$  at  $60 \text{ mm/s}$  printing speed.
- Support angle values were analysed and the optimal results were achieved at  $30^\circ$ . The maximal Charpy energy absorption was obtained as  $0.803 \text{ kJ/m}^2$  at  $30^\circ$  support angle.
- Build orientation values showed extremely effective results on edge Charpy impact test data. When the build orientation is considered together with the notch type, the good results of the edge can be explained more because it is the surface that meets the impact load. The maximal Charpy impact energy absorption was obtained as  $0.841 \text{ kJ/m}^2$  at edge position.
- When Notch type was examined, the highest Charpy values were obtained in U type samples. The keyhole cut out also gave relatively good results. The maximal Charpy impact energy absorption was obtained as  $0.827 \text{ kJ/m}^2$  at U notch type.
- As the filling type, the full filling type showed the best results compared to the mesh filling type. The maximal Charpy impact energy absorption was obtained as  $0.777 \text{ kJ/m}^2$  at full infill type.
- In DL, adam was applied as the optimization algorithm and tanh as the activation func. The number

of hidden layer in the runs that gave good results in the analysis was 3. 10% of the data was used for testing. DL, MSE value was calculated as 0.000923 and r square value as 0.97427.

- The activation func. utilized in ELM is sigmoid for input and linear for output. In ELM, the best (MSE) results were obtained with 180 neurons in the hidden layer (OP-ELM). In ELM, the best MSE result was calculated as 0.00173 and  $r^2$  value as 0.96178. The results showed that the OP-ELM optimization algorithm resulted in an effective ELM model when the activation function was in the sigmoid.
- For the models put forward this study, although the DL results are relatively better, it shows that both DL and ELM give very successful prediction results as the effective optimization. It is concluded that different artificial intelligence methods can be applied to optimize the outputs obtained with different parameters in each case.

## Acknowledgements

Due to the great earthquakes that occurred in Turkey on February 6 and turned our lives upside down; I would like to express my gratitude and gratitude to the Deanship and management of 19 Mayıs University Faculty of Engineering for the academic working environment and opportunities they provided us.

## Conflict of Interest Statement

The authors declare that there is no conflict of interest

## Data availability

All the raw data of analysis are available as supplementary data. Any other data generated or analyzed during this study are available from the corresponding authors on reasonable request.

<https://docs.google.com/spreadsheets/d/1cixYHjxhKUULWqhSZXMj9zqqpahjtSH9/edit?usp=sharing&ouid=104439447976128858155&rtopof=true&sd=true>

## References

- [1] G. D. Goh, S. Agarwala, G. L. Goh, V. Dikshit, S. L. Sing, and W. Y. Yeong, "Additive manufacturing in unmanned aerial vehicles (UAVs): Challenges and potential," *Aerospace Science and Technology*, vol. 63, pp. 140–151, 2017, doi:10.1016/j.ast.2016.12.019
- [2] M. D. Monzón, Z. Ortega, A. Martínez, and F. Ortega, "Standardization in additive manufacturing: activities carried out by international organizations and projects," *The International Journal of Advanced Manufacturing Technology*, vol. 76, no. 5–8, pp. 1111–1121, 2015, doi:10.1007/s00170-014-6334-1
- [3] C. Palanisamy, R. Raman, and P. kumar Dhanraj, "A review on mechanical properties of polyjet and FDM printed parts," *Additive Manufacturing*, vol. 79, no. 9. Springer Berlin Heidelberg, 2022. doi:10.1007/s00289-021-03899-0
- [4] S. Singh, S. Ramakrishna, and R. Singh, "Material issues in additive manufacturing: A review," *Journal of Manufacturing Processes*, vol. 25, pp. 185–200, Jan. 2017. doi:10.1016/j.jmapro.2016.11.006
- [5] S. Pattnaik, P. K. Jha, and D. B. Karunakar, "A review of rapid prototyping integrated investment casting processes," *Proceedings of the Institution of Mechanical Engineers, Part L: Journal of Materials: Design and Applications*, vol. 228, no. 4, pp. 249–277, Oct. 2014. doi:10.1177/1464420713479257
- [6] N. Anwer, B. Schleich, L. Mathieu, and S. Wartzack, "From solid modelling to skin model shapes: Shifting paradigms in computer-aided tolerancing," *CIRP Annals - Manufacturing Technology*, vol. 63, no. 1, pp. 137–140, 2014. doi:10.1016/j.cirp.2014.03.103
- [7] S. H. Chiu, K. T. Chen, S. T. Wicaksono, J. R. Tsai, and S. H. Pong, "Process parameters optimization for area-forming rapid prototyping system," *Rapid Prototyping Journal*, vol. 21, no. 1, pp. 70–78, Jan. 2015. doi:10.1108/RPJ-12-2012-0114
- [8] K. L. Alvarez C., R. F. Lagos C., and M. Aizpun, "Investigating the influence of infill percentage on the mechanical properties of fused deposition modelled ABS parts," *Ingenieria e Investigacion*, vol. 36, no. 3, pp. 110–116, 2016. doi:10.15446/ing.investig.v36n3.56610
- [9] P. Mantada, R. Mendricky, and J. Safka, "Parameters influencing the precision of various 3D printing technologies," *MM Science Journal*, vol. 2017, no. December, pp. 2004–2012, 2017. doi:10.17973/MMSJ.2017\_12\_201776

- [10] R. V. Aroca, C. E. H. Ventura, I. De Mello, and T. F. P. A. T. Pazelli, "Sequential additive manufacturing: automatic manipulation of 3D printed parts," *Rapid Prototyping Journal*, vol. 23, no. 4, pp. 653–659, Jun. 2017. doi:10.1108/RPJ-02-2016-0029
- [11] L. Cheng, P. Zhang, E. Biyikli, J. Bai, J. Robbins, and A. To, "Efficient design optimization of variable-density cellular structures for additive manufacturing: theory and experimental validation," *Rapid Prototyping Journal*, vol. 23, no. 4, pp. 660–677, Jun. 2017. doi:10.1108/RPJ-04-2016-0069
- [12] A. Haryńska, H. Janik, M. Sienkiewicz, B. Mikolaszek, and J. Kucińska-Lipka, "PLA-Potato Thermoplastic Starch Filament as a Sustainable Alternative to the Conventional PLA Filament: Processing, Characterization, and FFF 3D Printing," *ACS Sustainable Chemistry and Engineering*, vol. 9, no. 20, pp. 6923–6938, 2021. doi:10.1021/acssuschemeng.0c09413
- [13] B. D. de Castro, F. de C. Magalhães, T. H. Panzera, and J. C. Campos Rubio, "An Assessment of Fully Integrated Polymer Sandwich Structures Designed by Additive Manufacturing," *Journal of Materials Engineering and Performance*, vol. 30, no. 7, pp. 5031–5038, 2021. doi:10.1007/s11665-021-05604-8
- [14] J. Andrzejewski, K. Grad, W. Wiśniewski, and J. Szulc, "The use of agricultural waste in the modification of poly(Lactic acid)-based composites intended for 3d printing applications. the use of toughened blend systems to improve mechanical properties," *Journal of Composites Science*, vol. 5, no. 10, 2021. doi:10.3390/jcs5100253
- [15] M. Q. Tanveer, A. Haleem, and M. Suhaib, "Effect of variable infill density on mechanical behaviour of 3-D printed PLA specimen: an experimental investigation," *SN Applied Science*, vol. 1, no. 12, p. 1701, Dec. 2019. doi:10.1007/s42452-019-1744-1
- [16] M. A. Caminero, J. M. Chacón, I. García-Moreno, and G. P. Rodríguez, "Impact damage resistance of 3D printed continuous fibre reinforced thermoplastic composites using fused deposition modelling," *Composites Part B: Engineering*, vol. 148, no. April, pp. 93–103, 2018. doi:10.1016/j.compositesb.2018.04.054
- [17] I. Fekete, F. Ronkay, and L. Lendvai, "Highly toughened blends of poly(lactic acid) (PLA) and natural rubber (NR) for FDM-based 3D printing applications: The effect of composition and infill pattern," *Polymer Testing*, vol. 99, 2021. doi:10.1016/j.polymertesting.2021.107205
- [18] S. Korga, M. Barszcz, and L. Zgryza, "The effect of the 3D printout filling parameter on the impact strength of elements made with the FDM method," *IOP Conference Series: Materials Science and Engineering*, vol. 710, no. 1, 2019. doi:10.1088/1757-899X/710/1/012027
- [19] H. Hadidi et al., "Low velocity impact of ABS after shot peening predefined layers during additive manufacturing," *Procedia Manufacturing*, vol. 34, pp. 594–602, 2019. doi:10.1016/j.promfg.2019.06.169
- [20] A. K. Sood, R. K. Ohdar, and S. S. Mahapatra, "Improving dimensional accuracy of Fused Deposition Modelling processed part using grey Taguchi method," *Materials and Design*, vol. 30, no. 10, pp. 4243–4252, Dec. 2009. doi:10.1016/j.matdes.2009.04.030
- [21] B. Ameri, F. Taheri-Behrooz, and M. R. M. Aliha, "Mixed-mode tensile/shear fracture of the additively manufactured components under dynamic and static loads," *Engineering Fracture Mechanics*, vol. 260, no. July 2021. p. 108185, 2022. doi:10.1016/j.engfracmech.2021.108185
- [22] D. R. Hetrick, S. H. R. Sanei, O. Ashour, and C. E. Bakis, "Charpy impact energy absorption of 3D printed continuous Kevlar reinforced composites," *Journal of Composite Materials*, vol. 55, no. 12, pp. 1705–1713, 2021. doi:10.1177/0021998320985596
- [23] S. Kontárová et al., "Printability, mechanical and thermal properties of poly(3-hydroxybutyrate)-poly(lactic acid)-plasticizer blends for three-dimensional (3D) printing," *Materials (Basel)*, vol. 13, no. 21, pp. 1–28, 2020. doi:10.3390/ma13214736
- [24] R. A. García-León, M. Rodríguez-Castilla, and W. Quintero-Quintero, "Experimental Analysis of Impact Resistance of 3D Polycarbonate and Nylon + Carbon Fiber Specimens," *Journal of Materials Engineering and Performance*, vol. 30, no. 7, pp. 4837–4847, 2021. doi:10.1007/s11665-020-05422-4
- [25] V. Figueroa-Velarde et al., "Mechanical and physicochemical properties of 3d-printed agave fibers/poly(Lactic) acid biocomposites," *Materials (Basel)*, vol. 14, no. 11, 2021. doi:10.3390/ma14113111
- [26] F. Ning, W. Cong, Y. Hu, and H. Wang, "Additive manufacturing of carbon fiber-reinforced plastic composites using fused deposition modeling: Effects of process parameters on tensile properties," *Journal of Composite Materials*, vol. 51, no. 4, pp. 451–462, 2017. doi: 10.1177/0021998316646169
- [27] N. Sa'ude, S. H. Masood, M. Nikzad, and M. Ibrahim, "Dynamic Mechanical Properties of Copper-ABS Composites for FDM Feedstock," *Int. J. Eng. Res. Appl.*, vol. 3, no. 3, pp. 1257–1263, 2013. [Online]. Available: <http://scholar.google.com/scholar?hl=en&btnG=Search&q=intitle:Dynamic+Mechanical+Properties+of+Copper-ABS+Composites+for+FDM+Feedstock#0>
- [28] M. Samykano, S. K. Selvamani, K. Kadirgama, W. K. Ngui, G. Kanagaraj, and K. Sudhakar, "Mechanical property of FDM printed ABS: influence of printing parameters," *The International Journal of Advanced Manufacturing Technology*, vol. 102, no. 9–12, pp. 2779–2796, 2019. doi:10.1007/s00170-019-03313-0
- [29] S. Abid, R. Messadi, T. Hassine, H. Ben Daly, J. Soulestin, and M. F. Lacrampe, "Optimization of mechanical properties of printed acrylonitrile butadiene styrene using RSM design," *The International Journal of Advanced Manufacturing Technology*, vol. 100, no. 5–8, pp. 1363–1372, 2019. doi:10.1007/s00170-018-2710-6

- [30] A. Garg, A. Bhattacharya, and A. Batish, "Chemical vapor treatment of ABS parts built by FDM: Analysis of surface finish and mechanical strength," *The International Journal of Advanced Manufacturing Technology*, vol. 89, no. 5-8, pp. 2175-2191, 2017. doi:10.1007/s00170-016-9257-1
- [31] S. Khabia and K. K. Jain, "Comparison of mechanical properties of components 3D printed from different brand ABS filament on different FDM printers," *Materials Today: Proceedings*, vol. 26, pp. 2907-2914, 2019. doi:10.1016/j.matpr.2020.02.600
- [32] S. Khabia and K. K. Jain, "Influence of change in layer thickness on mechanical properties of components 3D printed on Zortrax M 200 FDM printer with Z-ABS filament material & Accucraft i250+ FDM printer with low cost ABS filament material," *Materials Today: Proceedings*, vol. 26, pp. 1315-1322, 2019. doi:10.1016/j.matpr.2020.02.268
- [33] C. Szegedy *et al.*, "Going deeper with convolutions," *2015 IEEE Conference on Computer Vision and Pattern Recognition (CVPR)*, Boston, MA, USA, 2015, pp. 1-9, doi: 10.1109/CVPR.2015.7298594.
- [34] J. Redmon, S. Divvala, R. Girshick and A. Farhadi, "You Only Look Once: Unified, Real-Time Object Detection," *2016 IEEE Conference on Computer Vision and Pattern Recognition (CVPR)*, Las Vegas, NV, USA, 2016, pp. 779-788, doi: 10.1109/CVPR.2016.91.
- [35] H. Tercan and T. Meisen, "Machine learning and deep learning based predictive quality in manufacturing: a systematic review," *Journal of Intelligent Manufacturing*, vol. 33, no. 7, pp. 1879-1905, Oct. 2022. doi:10.1007/s10845-022-01963-8
- [36] B. Ma, X. Ban, H. Huang, Y. Chen, W. Liu, and Y. Zhi, "Deep Learning-Based Image Segmentation for Al-La Alloy Microscopic Images," *Symmetry (Basel)*, vol. 10, no. 4, p. 107, Apr. 2018. doi:10.3390/sym10040107
- [37] P. Oborski and P. Wysocki, "Intelligent Visual Quality Control System Based on Convolutional Neural Networks for Holonic Shop Floor Control of Industry 4.0 Manufacturing Systems," *Advances in Science and Technology Research Journal*, vol. 16, no. 2, pp. 89-98, Apr. 2022. doi:10.12913/22998624/145503
- [38] W.-J. Lin, S.-H. Lo, H.-T. Young, and C.-L. Hung, "Evaluation of Deep Learning Neural Networks for Surface Roughness Prediction Using Vibration Signal Analysis," *Applied Sciences*, vol. 9, no. 7, pp. 1462, Apr. 2019. doi:10.3390/app9071462
- [39] Y. Pan, R. Kang, Z. Dong, W. Du, S. Yin, and Y. Bao, "On-line prediction of ultrasonic elliptical vibration cutting surface roughness of tungsten heavy alloy based on deep learning," *Journal of Intelligent Manufacturing*, vol. 33, no. 3, pp. 675-685, Mar. 2022. doi:10.1007/s10845-020-01669-9
- [40] Z. Li, Z. Zhang, J. Shi, and D. Wu, "Prediction of surface roughness in extrusion-based additive manufacturing with machine learning," *Robotics and Computer-Integrated Manufacturing*, vol. 57, no. October 2018, pp. 488-495, Jun. 2019. doi:10.1016/j.rcim.2019.01.004
- [41] N. Dimitriou *et al.*, "Fault Diagnosis in Microelectronics Attachment Via Deep Learning Analysis of 3-D Laser Scans," *IEEE Transactions on Industrial Electronics*, vol. 67, no. 7, pp. 5748-5757, Jul. 2020. doi:10.1109/TIE.2019.2931220
- [42] J. P. Yun, W. C. Shin, G. Koo, M. S. Kim, C. Lee, and S. J. Lee, "Automated defect inspection system for metal surfaces based on deep learning and data augmentation," *Journal of Manufacturing Systems*, vol. 55, no. May 2019, pp. 317-324, Apr. 2020. doi:10.1016/j.jmsy.2020.03.009
- [43] J. Zhang, P. Wang, and R. X. Gao, "Deep learning-based tensile strength prediction in fused deposition modeling," *Computers in Industry*, vol. 107, pp. 11-21, May 2019. doi:10.1016/j.compind.2019.01.011
- [44] A. Essien and C. Giannetti, "A Deep Learning Model for Smart Manufacturing Using Convolutional LSTM Neural Network Autoencoders," *IEEE Transactions on Industrial Informatics*, vol. 16, no. 9, pp. 6069-6078, Sep. 2020. doi:10.1109/TII.2020.2967556
- [45] G. Serin, B. Sener, A. M. Ozbayoglu, and H. O. Unver, "Review of tool condition monitoring in machining and opportunities for deep learning," *The International Journal of Advanced Manufacturing Technology*, vol. 109, no. 3-4, pp. 953-974, Jul. 2020. doi:10.1007/s00170-020-05449-w
- [46] Q. Wang, W. Jiao, P. Wang, and Y. Zhang, "A tutorial on deep learning-based data analytics in manufacturing through a welding case study," *Journal of Manufacturing Processes*, vol. 63, pp. 2-13, Mar. 2021, doi:10.1016/j.jmapro.2020.04.044
- [47] L. Cardoso Silva *et al.*, "Benchmarking Machine Learning Solutions in Production," in *2020 19th IEEE International Conference on Machine Learning and Applications (ICMLA)*, pp. 626-633, Dec. 2020. doi:10.1109/ICMLA51294.2020.00104
- [48] S. Klein, S. Schorr, and D. Bähre, "Quality Prediction of Honed Bores with Machine Learning Based on Machining and Quality Data to Improve the Honing Process Control," *Procedia CIRP*, vol. 93, pp. 1322-1327, 2020. doi:10.1016/j.procir.2020.03.055
- [49] G. Huang, T. Liu, Y. Yang, Z. Lin, S. Song, and C. Wu, "Discriminative clustering via extreme learning machine," *Neural Networks*, vol. 70, pp. 1-8, Oct. 2015. doi:10.1016/j.neunet.2015.06.002
- [50] G. Huang, G. Bin Huang, S. Song, and K. You, "Trends in extreme learning machines: A review," *Neural Networks*, vol. 61, pp. 32-48, 2015. doi:10.1016/j.neunet.2014.10.001
- [51] T. Liu, C. K. Liyanaarachchi Lekamalage, G. Bin Huang, and Z. Lin, "Extreme Learning Machine for Joint Embedding and Clustering," *Neurocomputing*, vol. 277, pp. 78-88, 2018. doi:10.1016/j.neucom.2017.01.115

- [52] Y. Wang, Z. Xie, K. Xu, Y. Dou, and Y. Lei, "An efficient and effective convolutional auto-encoder extreme learning machine network for 3d feature learning," *Neurocomputing*, vol. 174, pp. 988–998, 2016. doi:10.1016/j.neucom.2015.10.035
- [53] Z. Chen, D. Li, and W. Zhou, "Process parameters appraisal of fabricating ceramic parts based on stereolithography using the Taguchi method," *Proceedings of the Institution Mechanical Engineers, Part B: Journal Engineering Manufacture*, vol. 226, no. 7, pp. 1249–1258, Jul. 2012. doi:10.1177/0954405412442607
- [54] C. Palanisamy, R. Raman, and P. kumar Dhanraj, "Additive manufacturing: a review on mechanical properties of polyjet and FDM printed parts," *Polymer Bulletin*, vol. 79, no. 9, pp. 7065–7116, Sep. 2022. doi:10.1007/s00289-021-03899-0
- [55] M. Ramesh and K. Panneerselvam, "Mechanical investigation and optimization of parameter selection for Nylon material processed by FDM," *Materials Today: Proceedings*, vol. 46, pp. 9303–9307, 2019. doi:10.1016/j.matpr.2020.02.697
- [56] K. Raney, E. Lani, and D. K. Kalla, "Experimental characterization of the tensile strength of ABS parts manufactured by fused deposition modeling process," *Materials Today: Proceedings*, vol. 4, no. 8, pp. 7956–7961, 2017. doi:10.1016/j.matpr.2017.07.132

---

This is an open access article under the CC-BY



license